Employing Paramagnetic Shift for Responsive MRI Probes

Alice C. Harnden,[a] David Parker[a] and Nicola J. Rogers[b*]

[a] Department of Chemistry, Durham University, South Road, Durham DH1 3LE, UK
[b] Department of Chemistry, University of Warwick, Coventry, CV4 7AL, UK
*corresponding author

Abstract

Paramagnetic metal ions with anisotropic magnetic susceptibilities can shift the proton NMR signals of chelating ligands beyond the diamagnetic range of endogenous proton resonances. Such large shifts, along with enhanced longitudinal relaxation rates, allow paramagnetic complexes to be exploited as molecular imaging probes for MRI. Paramagnetically-shifted imaging probes are detected directly against zero background, as opposed to the indirect induced relaxation enhancement of surrounding water molecules, and are reviewed herein. The development of 'smart' probes that are sensitive to their surrounding environment is also being developed, and some of the challenges faced for in vivo imaging are discussed, including issues of sensitivity and dose, biodistribution and clearance. Several examples of lanthanide complexes have been investigated, and more recently certain paramagnetic transition metal complexes are being considered as potential imaging agents.

Keywords
imaging; responsive; paramagnetic; lanthanides; MRI; hyperfine shift

1. Introduction

Magnetic resonance imaging (MRI) is an important diagnostic tool for medicine and biomedical research due to its ability to image soft tissue both non-invasively and with high 3D spatial resolution. The development of MRI contrast agents has dramatically improved the information that can be garnered from MRI imaging, and gadolinium(III) complexes are used routinely in the clinic, increasing signal per unit time by enhancing the T_1 relaxation rates of proximal water molecules selectively [1]. However, this indirect method of tracing probe location is concentration dependent, whilst the biodistribution of contrast agents is usually heterogeneous, and relatively high doses, ca 0.1 mmol/kg^{-1} are required. *Direct* detection of a proton-containing tracer molecule is possible by MRI, even within the intense endogenous signals from water and fats in the body, by exploiting the paramagnetic shift phenomenon encountered in metal complexes with an anisotropic magnetic susceptibility. The reporter signal can be shifted away from the diamagnetic window, allowing its visualisation against a zero background (Figure 1).

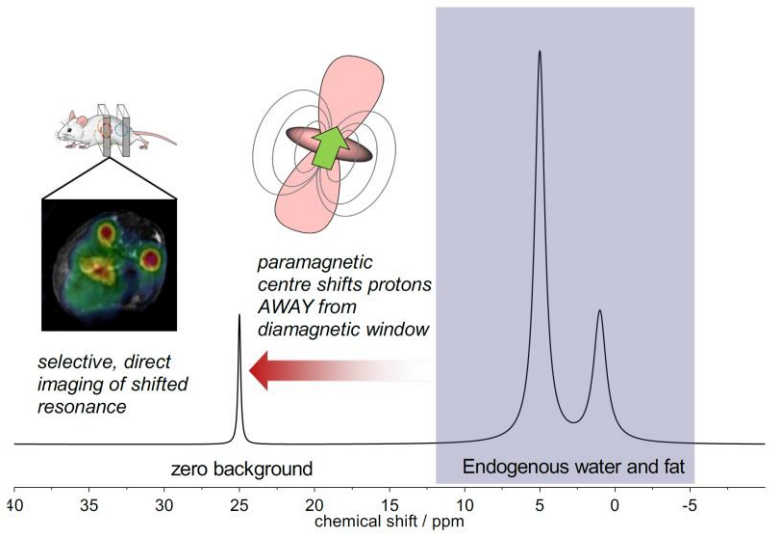

Figure 1. *Imaging paramagnetically-shifted proton signals against zero background signal in the body.*

Such an approach is analogous to heteronuclear MRI (^{31}P, ^{19}F, ^{13}C, ^{15}N, ^{7}Li and ^{23}Na), without the concomitant sensitivity issues and requirement for specialist imaging coils associated with non-proton MRI [2].

2. Paramagnetic Induced Chemical Shifts

The effect of paramagnetic species on NMR signals has been noted since the very beginnings of NMR [3–6]. In the 1950s, Bloembergen and Dickinson observed unexpected shifts in the NMR resonances of paramagnetic solutions, and subsequently suggested that *some* paramagnetic ions possess magnetic anisotropy, i.e. the magnitude of the electron-induced magnetic susceptibility varies with orientation [7]. A nucleus 'sees' the time-averaged magnetic moment of unpaired electrons, which is non-zero when the populations of the electronic states are not equal to one another. Such a situation occurs when there is a Boltzmann distribution across different low-lying energy states, e.g. across the crystal-field splitting in the *J* manifold in *f*-block compounds, or due to zero-field splitting and spin-orbit coupling in *d*-block systems.

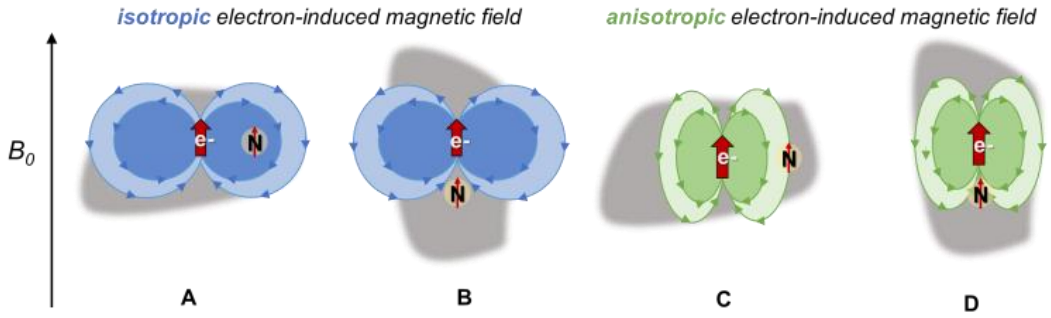

Figure 2. *The nucleus 'N' feels the dipolar magnetic field of an unpaired electron 'e-', which experiences extra field that subtracts (A, C) or adds (B, D) to the external field. Rotational motion averages these to zero for isotropic fields (A, B) but to non-zero for anisotropic fields (C, D).*

Unpaired electrons of paramagnetic compounds can therefore produce a large, temperature-dependent contribution to the observed shift (δ_{obs}) of a nucleus, which adds to the orbital diamagnetic (δ_{dia}) term, and is often referred to as the hyperfine shift (δ_{HF}). Although there are many possible contributions to δ_{HF}, only the pseudocontact term (δ_{PCS}) and/or the Fermi contact term (δ_{FCS}) are usually considered, as other contributions are negligible.

$$\delta_{obs} = \delta_{dia} + \delta_{FCS} + \delta_{PCS} \qquad (1)$$

The pseudocontact term describes the dipolar interaction (through-space), and the Fermi contact contribution describes the direct shielding constant experienced, due to a fraction of the unpaired electron spin density present actually at the nucleus of interest, either by direct delocalisation through σ–/π–bonds, or via spin polarisation. This term is important for atoms directly bonded to the paramagnetic centre, but is rapidly attenuated with the number of separating bonds [8].

The ability of lanthanide(III) complexes to induce large paramagnetic shifts was used by Hinckley in 1969 [9], and the physical origins were rationalised by Bleaney several years later [10], describing the effects of magnetic anisotropy on the observed NMR shifts in lanthanide complexes. Due to the large anisotropy of the magnetic susceptibility, short electronic relaxation times and predictable coordination chemistry of the trivalent lanthanides, they offer a great deal of potential as paramagnetic ions for NMR applications. The early 1970s saw an increased interest in the systematic application of paramagnetic shift reagents as tools for the organic chemist to elucidate NMR spectra of molecules with a large number of overlapping resonances [11,12]; indeed, enantiomerically pure lanthanide complexes have since been used as chiral shift reagents [13,14]. Paramagnetic shift agents have also been employed for solid state protein structural elucidation [15,16], and have been investigated as potential in vivo shift agents for $^{23}Na^{+}$ [17].

Paramagnetically shifted proton signals, such as nuclei in the local chelating ligand structure of a paramagnetic metal centre, can resonate at frequencies significantly shifted away from the usual diamagnetic range, enabling PARAmagnetically SHIFTed MRI probes, coined 'PARASHIFT' probes, to be imaged in vivo [18]. Paramagnetic-induced hyperfine shifts have also been exploited in the field of Chemical Exchange Saturation Transfer (CEST) imaging over the last 20 years [19–21], although the long scan times, continual irradiation with saturating frequencies, and problems associated with field inhomogeneity, limit the potential use of 'PARACEST' in humans. Notably, the rise in applications of paramagnetic complexes has also pushed advances in the development of more elaborate theoretical approaches for the calculations of hyperfine shifts, that go beyond the assumptions of Bleaney's theory [22–28].

3. PARASHIFT Probes for Imaging

PARASHIFT molecular probes need to be water soluble, stable in solution, and non-toxic at the imaging concentrations used, in order to be applicable in vivo. It is imperative that PARASHIFT probes are kinetically and thermodynamically stable with respect to metal ion dissociation, as much like free Gd^{3+}, other free Ln^{3+} ions are highly toxic and can trans-metallate in the body [29]. Compared with other imaging techniques (nuclear imaging, luminescence imaging) MRI is insensitive. Thus, it is important to maximise the signal-to-noise ratio (SNR) in the probe design. Ideally, the reporting proton resonance must be shifted as far away as possible from the endogenous protons so that a large excitation bandwidth can be used to allow the use of fast imaging sequences [18]. The reporter group must also provide a large single NMR signal, and therefore it is important to consider the symmetry, assess the possibility of forming diastereoisomers, and study the exchange dynamics of potential imaging resonances [30]. In addition to the hyperfine shift, paramagnetic centres can also enhance the relaxation rates of surrounding nuclei, which can be exploited to enhance sensitivity. The paramagnetic induced nuclear relaxation can give rise to rapid longitudinal relaxation rates, R_1 (i.e. $1/T_1$), facilitating fast-pulsed NMR techniques [31]. The linewidth of the reporting resonance, however, needs to be narrow to avoid SNR losses due to T_2 and the ratio R_1/R_2 should be as close to unity as possible [18,31,32].

One of the first examples of chemical shift selective imaging with a paramagnetic complex was published in 1996 by Aime, Botta and co-workers, using the complex $[YbL^1]^-$, known as YbDOTMA [33]. The intense C_4-symmetric methyl ^1H signal, at -14 ppm (27°C, 4.7 T, R1 = 15 s^{-1}, R_2 ~ 30 s^{-1}, was imaged selectively in phantoms at 4.7 T (200 MHz), using a 2D spin echo with 5 ms sinc pulse. This first proof-of-concept study successfully demonstrated that paramagnetic complexes could be imaged selectively in the presence of water at physiologically relevant concentrations (LD_{50} = 10.5 mmol/kg) (Figure 3). However, the 2D single slice imaging experiment took over 6 h to observe signal from the 3 mM solution.

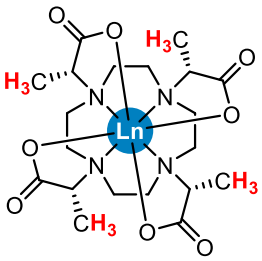

[LnL^1]$^-$
Ln = Yb, Tm, Pr, Tb, Dy

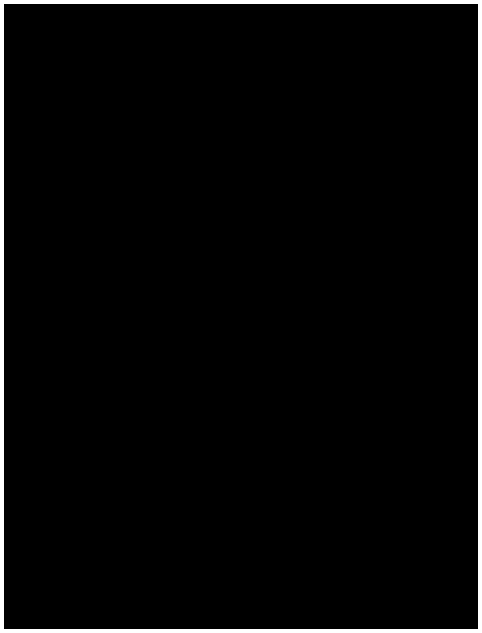

Figure 3 *(Left) Structure of [LnL^1], (LnDOTMA)$^-$ (Right) Adapted from reference* [33]. *2D spin echo chemical shift selective image of a phantom containing a series of aqueous solutions of [YbL^1]$^-$ from 0-100 mM. A 5 ms sinc pulse was used for the 90^o pulse and the transmitter offset was placed on the methyl group of interest to give the chemical shift selection. A 5 ms sinc pulse in the presence of a gradient was used for the 180 ^{o} pulse, giving slice selection. Slice thickness 4.5 mm, echo time 23 ms, relaxation delay = 0.15 s, number of phase encoding steps = 64, number of complex pairs = 128, number of transients = 2048. In plane spatial resolution = 0.625 mm × 0.625 mm (voxel size ca 1.8 mm^3). Copyright © (1996) Wiley-Liss, Inc., A Wiley Company.*

The NMR properties of other [Ln.L^1]$^-$ complexes were investigated by Bansal and co-workers, and [TmL^1]$^-$ was deemed the most suited to chemical shift selective imaging, with its sharp methyl resonance at -100 ppm (35°C) [34]. In 2014 Faber et al. successfully employed [TmL^1]$^-$ in cell-labelling studies in vivo; the complex was internalised into HT-1080 (human fibrosarcoma) cells prior to injection, and tracked by MRI in mice for 8 days, at an equivalent dose of ca. 1.6 mmol kg^{-1} [35] .

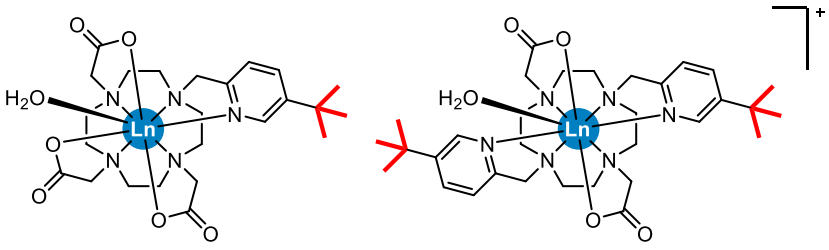

[Ln.L^2] **[Ln.L^3]$^+$**

Ln = Gd, Tb, Dy, Ho, Er, Tm, Yb

Figure 4 *Structures of carboxylate Ln PARASHIFT probes optimised for imaging*

In 2013, Parker and co-workers began to investigate the optimisation of a series of PARASHIFT lanthanide complexes, analysing both shift and relaxation properties, to inform judicious design of imaging probes [18]. Imaging sensitivity relies on the reporter group structure, its shift and relaxation properties [36]; PARASHIFT probes were designed with a *tert*-butyl reporter group placed about 6.5 to 7 Å from the lanthanide(III) ion enclosed within a cyclen-based macrocycle ([LnL^2] and [LnL^3]$^+$, Figure 4) to optimise fast longitudinal relaxation, whilst negating SNR losses to T_2 [18,23]. The *tert*-butyl group provides nine, in [LnL^2], or eighteen, in [LnL^3]$^+$ magnetically equivalent ^{1}H nuclei, giving a relatively intense resonance between -20.5 and +10.8 ppm

(22°C) depending on the lanthanide and complex [18]. Preliminary in vivo PARASHIFT imaging was performed on renally intact mice administered with clinically relevant doses (0.03 mmol/kg) of $[DyL^3]^+$ by intravenous injection, at 7 T. Short echo times (4 ms) and a narrow excitation bandwidth of 5 kHz were used, to reveal $[DyL^3]^+$ within skeletal muscles [18]. In pursuit of better sensitivity, Parker and co-workers developed new PARASHIFT agents with reporter groups shifted much further and > 70 ppm from the water/fat signals so that shorter excitation pulses (i.e. wider excitation bandwidths) could be used. It was hypothesised that increasing the excitation bandwidth to 20 kHz would significantly speed up image acquisition [31]. The structural modification from carboxylate ($[LnL^2]$) to methylphosphinate ($[LnL^4]$, Figures 5 and 6) chelating pendants was found to have a dramatic effect on the *tert*-butyl resonance frequency (Figure 5) [23].

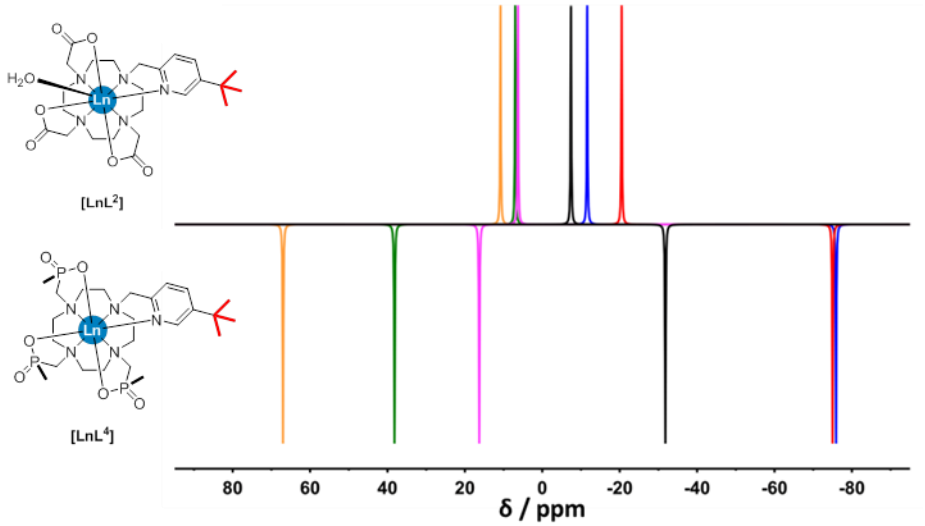

Figure 5. *Schematic representation of the experimentally measured chemical shifts of tert-butyl signals in $[LnL^2]$ (top) and $[LnL^4]$ (bottom) (D_2O, 22°C) (yellow – Tm, green – Er, magenta – Yb, black – Ho, red- Dy, blue –Tb.)*

The chemical shift range of the *tert*-butyl resonances in [LnL^4], 140 ppm (67 ppm [Tm] to -77 ppm [Tb]), is significantly larger than the range of [LnL^2]**,** 32 ppm (11 to -21 ppm), and further detailed studies of the hyperfine shift and relaxation properties of a range of tricarboxylate and triphosphinate 12-N-4 macrocyclic lanthanide complexes have shown that even small ligand variations can induce very large changes in the magnetic anisotropy [23,37]. The loss of the axially coordinating water molecule in the [LnL$_4$] systems (with respect to [LnL$_3$]) is associated with this drastic increase in both shift and relaxation [36,37]. The reason for the much larger shift of the *tert*-butyl group in the triphosphinate complexes [LnL^4] is the change in the orientation and size of the major axial component of the magnetic susceptibility tensor, which points directly towards the reporting *tert*-butyl resonance.[30] The *tert*-butyl proton signal of [DyL^4] (Figures 5 and 6) resonates at -75 ppm (22°C), > 20 kHz away from the water signal at 7 T and is therefore suitable for fast imaging sequences.

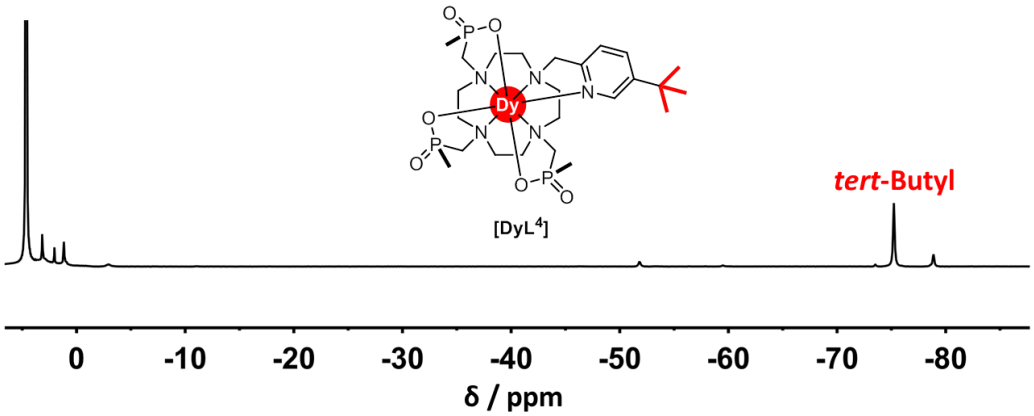

Figure 6. *^{1}H NMR spectrum and structure of [DyL^4] (D_2O, 9.4 T, 22°C), investigated in reference* [23]

The anionic bismethylphosphinate complex shown below ([DyL^5]$^-$, Figure 7), linked a carboxylate group close to the pyridine ring in order to improve its biodistribution with respect to the cationic analogue, i.e. a bismethylphosphinate complex similar to [LnL^3]$^+$. [38] [DyL^5]$^-$ was imaged in vivo with an optimised 3D gradient echo sequence at 7 T. The 18 proton tert-butyl NMR signal was excited at -60 ppm using a 20 kHz excitation bandwidth and much shorter echo times (TE = 1.45 ms, TR = 2.87 ms) and the image time was reduced to ca 60 s per 3D image (of 16 slices). An impressive detection limit of about 20 µmol/dm^3 was achieved at this temporal resolution, which allowed dynamic time series of images to be implemented to follow the kinetics of the molecular probe within the body, following the tail-vein injection of a single 0.04 mmol/kg dose of [DyL^5]$^-$ (Figure 7).

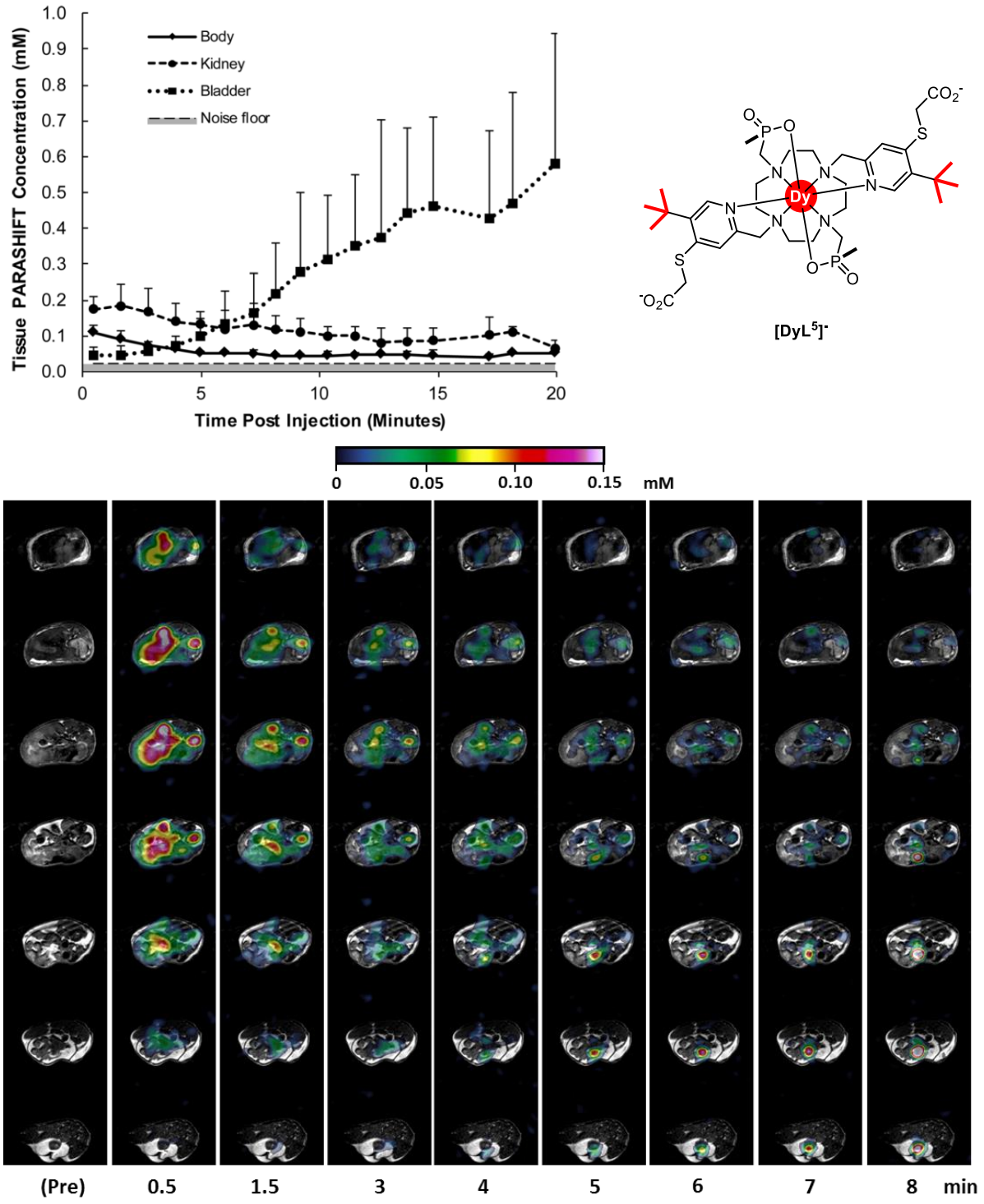

Figure 7. *From reference* [38] *with permission. (Top left) Time series analysis of PARASHIFT concentration from selected regions of interest in six mice. In vivo 3D gradient echo imaging of renally intact mice administered with 0.04 mmol/kg* $[DyL^5]^-$ *by intravenous tail vein injection. Imaged using 7 T preclinical MRI system with a 39 mm birdcage RF coil, TE= 1.45 ms, TR= 2.87 ms, 20 kHz excitation bandwidth, voxel sixe = 32* mm^3*, 62s per 3D image set (of 16 slices). (Top right) Structure of* $[DyL^5]^-$*. (Bottom) PARASHIFT signal from* $[DyL^5]^-$ *(colour scale) overlaid onto conventional structural MRI scans. Each column represents a different time point post injection. Within each column the data represent different spatial axial slices through the mouse. Copyright © (2016) The Authors Magnetic Resonance in Medicine published by Wiley Periodicals, Inc. on behalf of International Society for Magnetic Resonance in Medicine.*

Over the last 20 years several examples of PARASHIFT imaging have been reported using cyclen-based macrocyclic lanthanide complexes that are relatively simple to synthesise, mainly by the groups of Hyder [39–43] and Bansal [34,44,45], as well as optimised imaging probes synthesised by Parker and co-workers [38]. The magnitude of the paramagnetic shift is sensitive to physiological conditions including temperature, and efforts to convey functionality to these imaging probes has been exploited in spectroscopic imaging techniques, leading to sensing applications in vivo. These are described in more detail in the following section.

4. In vivo Sensing with PARASHIFT Probes

Selective excitation of PARASHIFT agents using 3D gradient echo MRI allows the spatial distribution of the probe to be determined, with the intensity of the signal in each pixel determining the image contrast. It is also possible to extract more information using magnetic resonance, than simply probe location, if the frequency of the PARASHIFT agent's reporting nuclei can change in response to their surrounding environment; MRS imaging (MRSI) is the spatial mapping of *spectroscopic information*, rather than simply probe concentration, and is often referred to as chemical shift imaging (CSI), spectroscopic imaging (SI), or multi-voxel spectroscopy. MRSI can be performed with responsive contrast agents, in order to map physiological parameters such as temperature, pH, and ion concentrations.

4.1. Temperature Sensing

The paramagnetic hyperfine shifts of PARASHIFT nuclei are inherently temperature dependent because magnetic anisotropy derives from the Boltzmann population of energy states. Therefore, the chemical shifts of protons within PARASHIFT complexes change with temperature. It is important to note that paramagnetic shifts are not necessarily expected to show a linear dependence with temperature, a T^{-2} dependency of the pseudo-contact shift is predicted for lanthanide ions based on Bleaney theory, for instance [10]. However, over small (physiological) temperature ranges an approximate linear dependence is observed and thus linear temperature coefficients are often quoted [46].

The most widely applied MRS thermometry method in the literature is the 'proton resonance frequency' technique, which exploits the temperature-dependent hydrogen-bonding of the water protons; the proton resonance exhibits a linear shift response to temperature, with a very small temperature coefficient of 0.01 ppm/°C [47,48]. This low thermal sensitivity limits the error of temperature measurements to ca 2°C [49], requires fat-suppression techniques, and is impractical for measuring small temperature differences in vivo. In 1996, $[YbL^1]^-$ (Figure 3) was proposed as a temperature-sensitive MRS probe and in vitro spectroscopic investigations of the methyl resonance revealed a linear -0.04 ppm/°C temperature coefficient, four-times greater than that of water [33]. Meanwhile, Hentschel and co-workers began to investigate the thermometry properties of $[PrL^6]$ (Figure 8) [50,51]; the methoxy group at -24.1 ppm (22°C, relative to the water signal) was selectively imaged in 10 mM phantoms, and a linear shift dependence with temperature of 0.13 ppm/°C was observed.

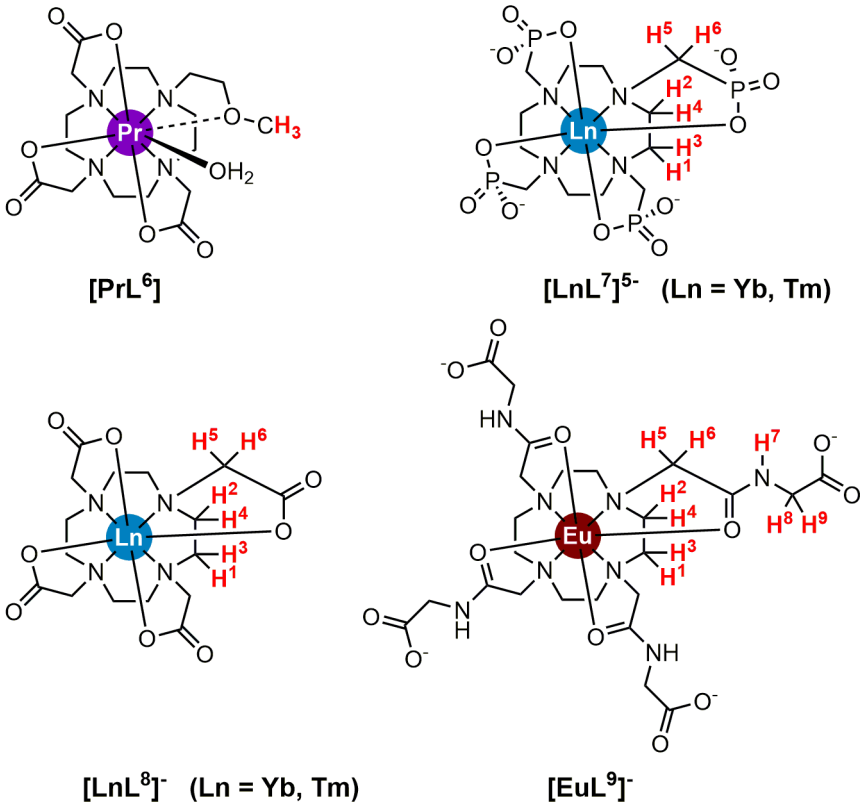

Figure 8. *Structures of selected temperature responsive MRS probes*

The methoxy shift was shown to be independent of pH and was used to measure the absolute temperature of the liver in a rat model, and verified by a rectal thermocouple (deviation < ± 1°C), although a high dose was required for this study (1 mmol/kg). Hentschel and co-workers later confirmed that the complex could be used to map temperature through the 2D spin echo spectroscopic imaging of phantoms [52–54].

A comparison of the NMR properties of $[YbL^1]^-$ with the analogous Pr, Tb, Dy and Tm complexes showed that $[TmL^1]^-$ had the greatest temperature coefficient, 0.57 ppm/°C, and its chemical shift was found to be insensitive to complex concentration, pH and the presence of Ca^{2+} ions [34]. $[TmL^1]^-$ was successfully employed for temperature mapping in rats with millimetre resolution, using a frequency selective pulse [40,44,45]. However, these studies relied on renal ligation and high doses of 1-2 mmol/kg in order to supress the fast clearance of $[TmL^1]^-$ via the kidneys. Despite the incredibly short half-life of $[TmL^1]^-$ in the blood (ca 7 min), Sled and co-workers managed to measure the internal temperatures of the aorta, inferior vena cava and kidney within this time window at 11.7 T, following a single bolus injections of 0.7 mmol/kg within physiologically intact mice [55].

It is becoming clear that the size and T-sensitivity of the resonant frequency of a paramagnetically shifted reporter resonance is a property of both the lanthanide ion and the ligand used to complex it. No longer can all-embracing theories, such as Bleaney's,[10] be invoked to rationalise, let alone predict behaviour.[22,23,28] For example, it has been noted that Tm complexes often produce much larger shifts with larger T coefficients that might have been expected. For many of these it is likely, and has been predicted[56] that the relative thermal population and anisotropy of the individual lanthanide ion m_J sub-states needs to be considered. Each m_J sub-level has a different magnetic susceptibility anisotropy: their relative order is determined by the ligand field[22] and their energy separation with respect to kT (2.5 kJ/mol at 298K) can strongly influence their weighted population and hence the T-dependence of the overall paramagnetic shift.[56]

Zuo *et al*. investigated the thulium(III) complex of the tetraphosphinate ligand, known as DOTP ($[TmL^7]^{5-}$, Figure 8) as a potential probe for MR thermometry [57] (notably, Ln^{3+} complexes of DOTP were originally studied as MR probes to distinguish intra- and extra- cellular concentrations of Na^+ in vivo, by ^{23}Na and ^{31}P MR imaging [17,58]).

The H_6 proton signal of $[TmL^7]^{5-}$ (Figure 8) resonates at -142 ppm (37°C) with a relatively narrow line width (ca 300 Hz at 7 T) and a significant linear temperature dependence of 0.89 ppm/°C, allowing greater thermal resolution than with $[TmL^1]^-$. Similarly to $[TmL^1]^-$ thermometry, the chemical shift of the $[TmL^7]^{5-}$ proton resonance is unaffected by pH (between 6.5 and 8.5), and in vivo thermometry has been demonstrated in renally ligated rats dosed with 1 mmol/kg of $[TmL^7]^{5-}$ [57]. However, the sensitivity of the complex to variations in Ca^{2+} concentration reduces the accuracy of temperature measurement in vivo.

The C_4 symmetric complex, $[LnL^8]^-$, (i.e. analogous lanthanide complexes of the commercial gadolinium contrast agent Dotarem [1], Figure 8) has also been employed successfully as an MSRI thermometry probe [59,60]; the $[TmL^8]^-$ H_5 resonance at -227 ppm (37°C) has a temperature coefficient of 0.91 ppm/°C, and is insensitive to variation of both pH and $[Ca^{2+}]$. In vivo temperature measurements were performed, at 9.4 T, on tumour-bearing mice infused with 1-2 mmol kg^{-1} $[TmL^8]^-$ and with scan times of ca 4 min [60]. Such a dose is generally regarded as being beyond the safe dose for analogous Gd MRI contract agents, and the ability to obtain fast temperature changes is limited by the acquisition time.

Tetra-amide based lanthanide(III) complexes have been thoroughly investigated for use in PARACEST imaging. The efficiency of CEST, i.e. detecting the signal loss of a pool of protons that are exchanging with a selectively saturated proton signal, depends upon the rate of exchange with respect to the chemical shift difference of the two proton pools, and is thus enhanced by large frequency differences. PARACEST agents tend to exploit exchangeable protons (i.e. NH, OH) within paramagnetic complexes, that are significantly shifted away from the bulk water signal with which they exchange. In 2011 Hyder [61,62], Sherry and co-workers investigated the possibility of dual modality MRI by combining PARACEST and PARASHIFT imaging techniques to detect the Eu(III) complex of the carboxylate-appended tetra-amide ligand ($[EuL^9]^-$, Figure 8) in phantom solutions [63]. In vitro experiments of 20 mM phantoms were performed, using MRSI to detect the non-exchangeable cyclen proton H_4, which has the largest temperature coefficient of 0.13 ppm/°C. Direct MRSI of $[EuL^9]^-$ revealed the concentration and temperature information per pixel, as a means to adjust subsequent CEST images for quantitative information, which image the molecule indirectly due to exchange with water. This in vitro experiment was performed at 11.7 T and required relatively high saturation powers for the CEST imaging, with both long MRSI (4.5 min) and CEST (7 min) imaging times.

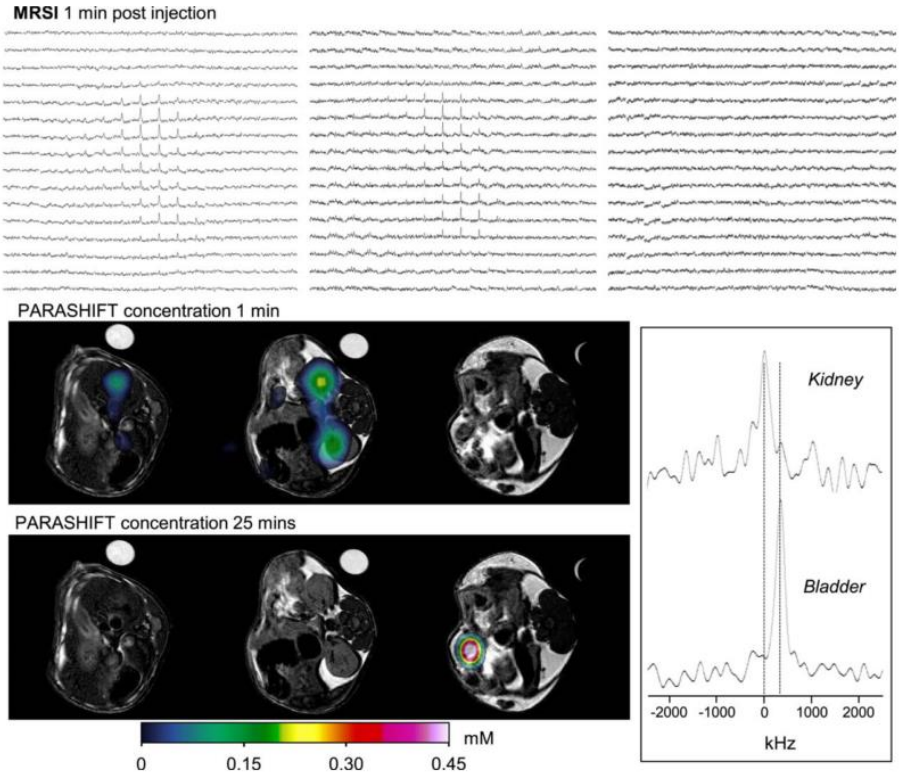

Figure 9. *From reference* [38] *with permission. In vivo spectroscopic imaging of renally intact mice administered with 0.04 mmol/kg* $[DyL^5]^-$ *by intravenous tail vein injection. (Top) Spectral grids for three of the MRSI slices acquired 1 minute after intravenous injection (Bottom left) Reconstructed PARASHIFT tissue distribution (derived from peak area for each voxel in 3DSI experiment) at 1 minute and 25 minutes post injection. (Bottom right) Spectra extracted from selected regions of interest. Imaged using 7 T preclinical MRI system with a 39 mm birdcage RF coil, TE= 0.73 ms, TR= 7.69 ms, 20 kHz spectral width, 63s per data set. Copyright © (2016) The Authors Magnetic Resonance in Medicine published by Wiley Periodicals, Inc. on behalf of International Society for Magnetic Resonance in Medicine.*

Parker and co-workers have successfully used MRSI of PARASHIFT agents to map temperature information [18,38,46]. MRSI was performed in vivo on renally intact mice, following intravenous injection of 0.04 mmol/kg of $[DyL^5]^-$ shown in Figure 9 (the temperature coefficient of the *tert*-butyl resonance was 0.28 ppm/°C in mouse plasma). A shift in the *tert*-butyl frequency between the bladder and the kidney were observed, indicating a 4°C difference in temperature between these organs, and imaging was performed at relatively high temporal resolution (63 s per image set) [38].

The intrinsic temperature sensitivity of paramagnetically shifted resonances has enabled the development of a new tool for in vivo temperature measurement. Accurate thermometry requires the temperature coefficient to be significant enough for high temperature resolution, without being too large to cause spatial distortions in the frequency encoding dimension. It is important that the reporter signal has a narrow linewidth, to ensure that chemical shift data can be readily extracted, and that it responds to temperature only, without shifting due to modulation of other external variables.

4.2. pH Sensing

Whilst the hyperfine shift of PARASHIFT agents has a dependence upon temperature, the chemical shift may also be sensitive to other external variables, such as pH, which can be exploited for MRI sensing. $[YbL^7]^{5-}$

(Figure 8) can protonate at all four of the phosphonate groups (equations 2-5), giving rise to a pH dependence of the proton resonance frequency [64]:

$[Yb(HL)]^{4-}$	⇌	$[YbL]^{5-}$	+	H^+	$pK_{a4} = 7.76$	(2)
$[Yb(H_2L)]^{3-}$	⇌	$[Yb(HL)]^{4-}$	+	H^+	$pK_{a3} = 6.56$	(3)
$[Yb(H_3L)]^{2-}$	⇌	$[Yb(H_2L)]^{3-}$	+	H^+	$pK_{a2} = 5.33$	(4)
$[Yb(H_4L)]^{-}$	⇌	$[Yb(H_3L)]^{2-}$	+	H^+	$pK_{a1} = 3.86$	(5)

The chemical shift separation between selected pairs of ^1H resonances was found to have a linear dependence that was negligibly affected by complex concentration, ionic strength and, most crucially, temperature; allowing for ratiometric measurement of pH. NMR measurements of pH were also achieved by Zuo and Sherry using $[TmL^7]^{5-}$, where it was found that H_6 (Figure 8) has a linear pH dependence between of -3.27 ppm/pH unit in the pH range 5.5 to 7.5, but was also temperature dependent [65]. A deconvolution of variables was therefore necessary to unravel the two different variables, using two different proton signals with different response coefficients to each variable using simultaneous equations (equations 6 and 7):

$$\Delta\delta(i) = C_T(i)\Delta T + C_{pH}(i)\Delta pH \quad (6)$$

$$\Delta\delta(j) = C_T(j)\Delta T + C_{pH}(j)\Delta pH \quad (7)$$

Where $C_T(i)$, $C_{pH}(i)$, $C_T(j)$, $C_{pH}(j)$ are the linear coefficients of the temperature and pH dependence of the chemical shifts in $[TmL^7]^{5-}$ as measured in vitro for protons i and j respectively. This technique was used to simultaneously measure the temperature and pH changes in live rats undergoing ultrasonic hyperthermia treatment, following local injection of 0.15 mmol/kg $[TmL^7]^{5-}$ [66]. Analysis of the chemical shifts of H_2 and H_6 (Figure 8) allowed temperature and pH mapping that was concurrent with inserted pH electrode and thermocouple measurements. Hyder et al. used a similar method to measure the brain temperature and pH of rats by focusing on two pairs of proton resonances either side of the water resonance [67,68]. Animals were renally ligated and injected with ca 1.5 mmol/kg of $[TmL^7]^{5-}$ and the resonances of each pairs of shifts were acquired separately from each other. Additional animal studies reduced the dose of complex to 1 mmol/kg and 2D CSI images of the brain (voxel size 10.2 µL) were obtained in 6 minutes [39]. The efficiency of the 2D mapping was improved and extended to 3D using spherical encoding instead of rectangular, which reduced the $[TmL^7]^{5-}$ dose to 0.5 mmol/kg, and increased the resolution (voxel size 1 µL) with 5 min scan times [41]. Extracellular pH maps of rat brains were generated in animals bearing 9L and RG2 tumours, and [42] the extracellular pH within tumours (7.0) was found to be lower than that in normal brain tissue (7.4), as can be seen below in the pH/T sensing experiment, Figure 10.

Figure 10. *From reference* [42] *with permission. Representative extracellular pH maps of rats bearing (A) 9L and (B) RG2 tumors. (i) T2-weighted image showing tumor localization (tumour = blue outline; brain = brown outline). (ii) A portion of the 3D chemical shift imaging (CSI) data for the slice in (i). (iii) Examples of spectra from intra-tumoural and peri-tumoural voxels. (iv) quantitative maps of the extracellular pH were obtained using multiple [TmL^{7}]$^{-}$ peaks and their respective pH sensitivities. Imaged using a 11.7 T horizontal-bore spectrometer, TR = 5 ms, 35 kHz spectral width. Copyright ©(2016) John Wiley and Sons, Ltd.*

The complex [TmL^{7}]$^{5-}$ was also used to map the effectiveness of temozolomide treatment (a chemotherapy drug) on U251 tumours by monitoring the pH of the tumour and brain [69], and demonstrated that the pH of both tumour and brain tissue was higher in treated rats. Although these studies demonstrate the successful use of [TmL^{7}]$^{5-}$ to map temperature and pH in vivo, high doses were required with renal ligation.

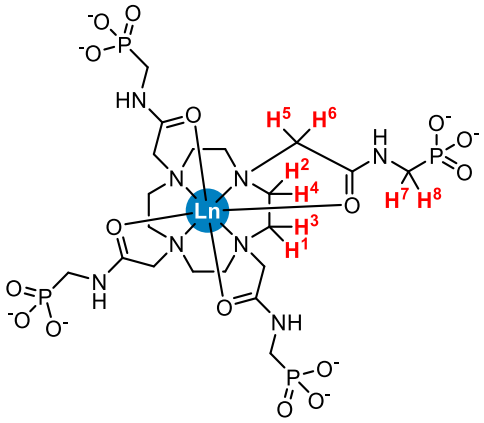

[LnL^{10}]$^{5-}$
where Ln = Gd, Yb, Tm

Figure 11*. Structure of [LnL^{10}]$^{5-}$*

The phosphonate-appended tetra-amide complex [GdL^{10}]$^{5-}$ (Figure 11) has been studied as a pH responsive T_1 contrast agent because the relaxivity of the complex is pH dependent [70–72]. The Yb^{3+} and Tm^{3+} complexes have been investigated as dual PARACEST and PARASHIFT probes [73]. The chemical shifts of the non-exchangeable resonances are pH dependent with the most sensitive measurement, 5.2 ppm/pH unit (35°C), arising from the difference between H_6 and H_8 in [TmL^{10}]$^{5-}$. This chemical shift difference also varies with temperature, 0.3 ppm/°C (35°C). Determination of pH and T simultaneously required two pairs of chemical shifts, H_6-H_8 and H_2-H_3, each with different pH/T sensitivities. Phantoms studies were used to compare the use of PARASHIFT and PARACEST in pH mapping which demonstrated that although CEST experiments could provide better spatial resolution PARASHIFT experiments had much higher pH sensitivities. High resolution pH mapping of [LnL^{10}]$^{5-}$ may be feasible using a combination of PARACEST and PARASHIFT techniques. However, further in vitro experiments are required to determine any sensitivities to cations, e.g. Ca^{2+}, Mg^{2+}, before in vivo capability can be realised.

Parker and co-workers sought to introduce pH responsive behaviour to their optimised PARASHIFT probes through the addition of a phosphonate group adjacent to the *tert*-butyl reporter group ([LnL^{11}]$^{-}$, Figure 12) [46]. The PARASHIFT *tert*-butyl resonance of the pH sensitive trimethylphosphinate (Ln(PMe$_3$)) probe was +74 ppm for the Tm^{3+} complex to -78 and -83 ppm for the Dy^{3+} and Tb^{3+} complexes respectively (22°C). The chemical shift of the reporter varies with pH (Figure 12) and pK_a values of [LnL^{11}]$^{-}$ averaged 7.16 (±0.06) in D_2O. The total shift range of this pH sensitivity and the linear temperature dependencies were both found to vary between lanthanides. The dual temperature and pH sensitivity of the probe means that the co-injection of two Ln^{3+} complexes is required to gain chemical information of tissues. Tm^{3+} and Dy^{3+} complexes were used for in vivo studies due to their large shift and similar longitudinal relaxation rates at 7 T. The two complexes were administered intravenously at 0.04 mmol/kg in renally intact mice. A triple imaging experiment allowed

simultaneous acquisition of the water signal and each of the well-separated *tert*-butyl signals and was achieved by dual, back-to-back RF pulses to excite the Dy and Tm complexes consecutively; a spectral width of 60 kHz was used to encompass all three signals. No specific excitation pulse was applied to the water resonance frequency as sufficient excitation was achieved with the two original pulses. Simultaneous equations can be solved for the chemical shift of the two *tert*-butyl resonances in order to extract the T and pH. These studies assessed the pH and temperature of the liver to be 7.1 and 34.5°C and the bladder to be 6.8 and 31°C.

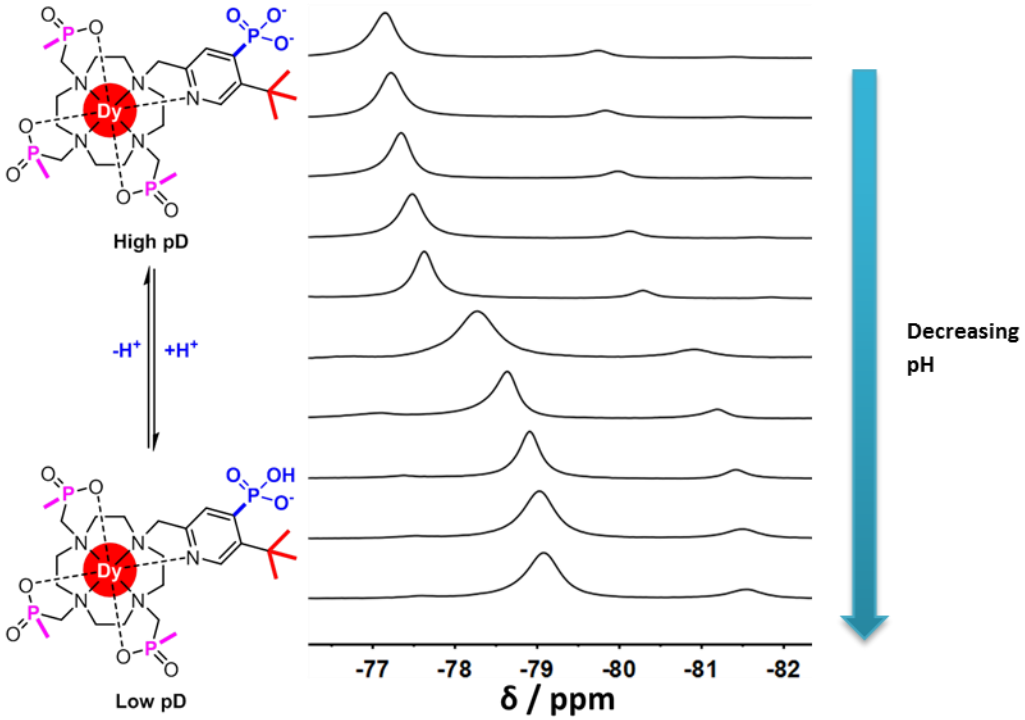

Figure 12. *Stacked ^{1}H NMR spectra of [DyL^{11}]$^{-}$ at varying pD (D_2O, 11.7 T, 22°C)*

Altered extracellular pH in vivo is associated with certain chronic diseases. There are very few non-invasive methods to quantify pH in vivo. ^{31}P MRS utilises the chemical shift of pH sensitive, phosphorus-containing metabolites, although the analogous use of pH sensitive ^{1}H metabolites is less well established. PARASHIFT molecular probes offer an alternative non-invasive MR technique, however the nature of the pH responsive group must be chosen carefully. The pK_a value must be within a biologically relevant range and should be insensitive to additional external variables, such as small changes in protein or local calcium or magnesium ion concentrations.

5. Important Practical Considerations for in vivo Imaging

Many examples of responsive PARASHIFT molecular probes have been employed successfully in imaging experiments, mainly with C_4-symmetric DOTA-type lanthanide complexes [TmL^{1}]$^{-}$ and [TmL^{7}]$^{5-}$, and *tert*-butyl appended Dy(III) and Tm(III) macrocyclic complexes. In order for PARASHIFT imaging to have clinical relevance however, it is important to consider the dose and method of administration required to produce adequate image sensitivity, as well as the pharmacokinetics/biodistribution of the molecular probe, and their interactions with other physiological species e.g. proteins and endogenous cations.

Most PARASHIFT agents studied to date suffer from fast clearance in the body, limiting the time-frame in which to image the molecular probe in organs other than the bladder to tens of minutes. Many early imaging studies were limited by the use of large doses (>0.1 mmol/kg, the clinical dose advised for DOTAREM), renally

ligated animals to eliminate clearance pathways, or continuous infusion of the PARASHIFT probe to maintain sufficient signal intensity.

Hyder et al. encapsulated $[TmL^7]^{5-}$ complex (Figure 8) in 1,2-dipalmitoyl-sn-glycerophosphocholine (DPPC) liposomes in order to enhance local concentrations, and the encapsulation process apparently had little effect on the chemical shifts of the $[TmL^7]^{5-}$ protons[74]. In vitro MRSI experiments suggested signal amplification could be achieved using nanomolar amounts of liposomes compared to free $[Tm.L^7]^{5-}$. Significant in vivo improvements in sensitivity have been achieved in more recent studies, more than 20-fold [38,46], with carefully designed complexes. Recently, investigation of the co-infusion of $[TmL^7]^{5-}$ with an anionic transport inhibitor showed enhanced probe concentrations, albeit with high infusion doses of 1 mmol/kg [43].

Strategies to enhance the sensitivity of these responsive probes have been considered. Greater signal intensity (SI) per unit time can be gained by working at higher field of course, but increasing the SI by maximising the local probe concentration has also been considered. These approaches include the use of multimeric complexes, where the probes are conjugated to a passive biocompatible entity,[75] or the use of non-covalently assembled adducts where the probes are locally concentrated inside a liposome or micelle.[74] Such higher molecular volume systems clear more slowly form the body, lengthening the detection window. In the future, conjugation to efficient and cheap targeting vectors can be envisioned, for example based on medium MW peptide carriers. Other approaches that can be employed to alter the pharmacokinetics involve changing the chemistry of the molecular probe; Parker found that anionic PARASHIFT complexes cleared slightly more slowly than cationic complexes,[18,38] and both Parker and Hyder sought to reduce clearance rates by increasing the size of the molecular probe by conjugation to biopolymers [75] or developing dendrimers containing $[TmL^1]^-$ [76]. Unfortunately, Hyder et al found that the loss of the C_4 structural symmetry resulted in the loss of sharp resonances and severe signal broadening was observed as the dendrimers increased in size.

The phosphonate groups in compounds such as $[LnL^7]^{5-}$ and $[LnL^{10}]^{5-}$ are known to bind divalent metal ions, often forming stable adducts, and interferences from interactions with Ca^{2+} ions within the body may pose a problem for in vivo imaging [77]. Although some studies have considered the effect of Ca^{2+} concentration [39], absolute determination of pH and/or T in vivo is impractical using these probes. Furthermore, injection of $[LnL^7]^{5-}$ leads to a drop in blood pressure as it binds to available cations in the blood [78].

Hudson and Milne modified the tetra-amide structure of $[EuL^9]^{5-}$ with propargyl arms to prevent problems with Ca^{2+} binding and the chemical shifts were found to be independent of both pH and $[Ca^{2+}]$. However, this renders the complex tricationic, which may give rise undesirable biodistribution and toxicity issues. The temperature sensitivity (1.76 ppm/°C) was reproducible when performed in pseudo-biological conditions, but no in vivo studies were reported [79]. Similarly, in control experiments in vitro, the pH and T sensitivity of complexes of $[LnL^{11}]$ has been shown to be independent to variation of both Mg and Ca ion concentrations, over the range 0.5 to 5 mM.[46]

5.1. Towards Non-Lanthanide PARASHIFT agents

The medical community routinely use Gd-based contrast agents for MRI, but in 2006 links to the rare but severe illness nephrogenic systemic fibrosis were found [80], and in 2017 the European Medicines Agency has documented gadolinium accumulation in patients' brain tissue, leading to restrictions in the use of the most commonly used contrast agent, $[Gd.DTPA]^{2-}$ [81]. PARASHIFT agents have the potential for better sensitivity than conventional relaxivity Gd^{3+} contrast agents because they are imaged directly, against zero background, and therefore lower concentrations of lanthanide complexes can be used for imaging studies. There has also

been an impetus to look towards *d*-block metals to replace gadolinium contrast agents [82–84], and more recently the search for new PARASHIFT agents based on paramagnetic d-block systems.

Morrow and co-workers have synthesised stable Fe(II) and Co(II) complexes using 9-N-3 and 12-N-4 based ligands appended with 6-methyl-2-picolyl groups (Figure 13). These six-coordinate aza-macrocyclic based ligands were found to stabilise the high-spin forms of Fe(II) and Co(II) due to the weaker ligand field produced as a result of the steric demand of the 6-methyl substituted pyridines. The complexes are paramagnetic with an anisotropic magnetic susceptibility that gives a relatively large hyperfine shift [85–87]; for example the proton signals within 12-N-4-based Fe(II) and Co(II) complexes span the range +300 to −80 ppm, compared to LnDOTA signals that span +300 to −500 ppm [Dy] and +400 to −300 ppm [Tm].[88] The transition metal complexes $[ML^{12}]^{2+}$ and $[ML^{13}]^{2+}$ were found to be kinetically inert in biological media and the chemical shifts are insensitive to pH (within physiological range) and biological ions (PO_3^{4-}, CO_3^{2-}, Zn^{2+}, Ca^{2+}). Linear temperature dependence was observed for all complexes and the largest temperature coefficient was 0.52 ppm/°C for $[Co(TMPC)]^{2+}$.

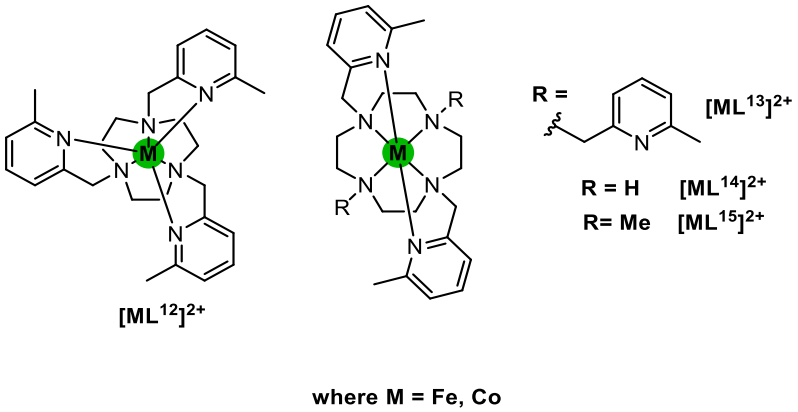

Figure 13. *Structures of 9-N_3 and 12-N_4 transition metal based PARASHIFT probes*

More recently, the methyl groups in the di- picolyl complexes $[ML^{14}]^{2+}$ and $[ML^{15}]^{2+}$ have been investigated (Figures 13 and 14) [87]. $[ML^{14}]^{2+}$ exhibited similar MR properties to the tetra- picolyl, $[ML^{13}]^{2+}$. The picolyl-methyl shifts of all complexes were shifted well outside the diamagnetic region, between -22 and -113 ppm (25°C). The additional methyl groups in $[ML^{15}]^{2+}$ were found to shift in the opposite direction to the picolyl-methyls (Figure 14). The presence of two highly shifted resonances could allow for more accurate temperature measurements and the temperature coefficients ranged from 0.1 to 0.58 ppm/°C. However, for both Co^{2+} complexes the linewidths of the methyl resonances were extremely broad, reducing the potential for use in vivo. The linewidths of the analogous Fe complexes were significantly narrower, but were less further shifted.

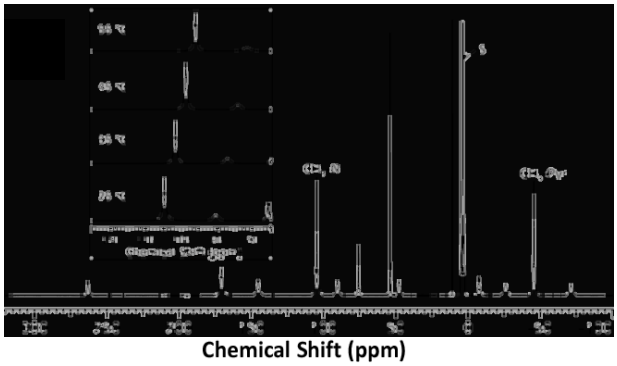

Figure 14. *Adapted from reference* [87] *with permission.* ^{1}H *NMR of* $[FeL^{15}]^{2+}$ *at 100 mM NaCl in* D_2O*, pD 7.2, at 25 °C for 10 mM complex. The proton resonances of pyridine and N-methyl groups on 12-*N_4 *are labelled* CH_3*-Pyr and* CH_3*-N, respectively. Solvent peak is labelled "S". Inset shows the effect of increasing temperature on the* ^{1}H *resonance of N-*CH_3*. Copyright © (2018) The Royal Society of Chemistry.*

New and co-workers have also developed a Co(II) based PARASHIFT complex that exhibits distinctive NMR responses to anions in aqueous solution [89]. The paramagnetically shifted *N*-Me resonance of $CoMe_6TrenCl$ was observed to give a distinctive spectral profile within the 180-130 ppm region upon reversible binding of fluoride, citrate, lactate and acetate.

Despite these in vitro spectroscopic studies with *d*-block PARASHIFT complexes, currently no imaging studies have been reported to date and cobalt toxicity may be an issue for Co-based probes; optimised probes for imaging have not yet been designed, and little has been done in terms of modelling the shift and relaxation properties of paramagnetic *d*-block systems, where the contact shift is more significant due to an increase in spin delocalisation onto the ligand in coordination systems [90–93].

6. Conclusions

Paramagnetic probes offer the chance to significantly increase the information that can be extracted non-invasively by MRI. Monitoring PARASHIFT resonances with MRSI techniques has significantly reduced scan times compared to diamagnetic MRSI and PARACEST imaging, and can be performed on a clinical scanner with no hardware modifications. Real-time monitoring and mapping of physiological processes can assist in the understanding and diagnosis of various diseases, and although only temperature and pH have been thoroughly investigated to date, careful selection of functional groups may enable the future monitoring of other useful biological markers such as cation concentration or enzyme activity.

Additional work on the conjugation of targeting vectors onto PARASHIFT probes may also increase the clearance times and enable specific tissues/organs/pathologies to be monitored in real time. It is likely that the first such studies will address imaging diseased kidneys and liver organs, as these are the simplest to address in this challenging work.

Acknowledgements

This work was supported by the ERC and EPSRC.

Conflicts of interest

Declarations of interest: none

References

[1] P. Caravan, J.J. Ellison, T.J. McMurry, R.B. Lauffer, Gadolinium(III) Chelates as MRI Contrast Agents: Structure, Dynamics, and Applications., Chem. Rev. 99 (1999) 2293–352. doi:10.1021/cr980440x.

[2] B. Ross, S. Bluml, Magnetic resonance spectroscopy of the human brain, Anat. Rec. 265 (2001) 54–84. doi:10.1002/ar.1058.

[3] B. V. Rollin, Nuclear Magnetic Resonance and Spin Lattice Equilibrium, Nature. 158 (1946) 669–670. doi:10.1038/158669a0.

[4] B. V. Rollin, J. Hatton, Nuclear Magnetic Resonance at Low Temperatures, Nature. 159 (1947) 201–201. doi:10.1038/159201a0.

[5] N. Bloembergen, E.M. Purcell, R. V. Pound, Relaxation effects in nuclear magnetic resonance absorption, Phys. Rev. 73 (1948) 679–712. doi:10.1103/PhysRev.73.679.

[6] J.A. Jackson, J.F. Lemons, H. Taube, Nuclear magnetic resonance studies on hydration of cations, J. Chem. Phys. 32 (1960) 553–555. doi:10.1063/1.1730733.

[7] W.C. Bloembergen, N. Dickinson, On the Shift of the Nuclear Magnetic Resonance in Paramagnetic Solutions, Phys. Rev. 79 (1950) 179–180. doi:https://doi.org/10.1103/PhysRev.79.179.

[8] I. Bertini, C. Luchinat, G. Parigi, E. Ravera, Chapter 2 - The hyperfine shift, in: I. Bertini, C. Luchinat, G. Parigi, E. Ravera (Eds.), NMR Paramagn. Mol. (Second Ed., Second Edi, Elsevier, Boston, 2017: pp. 25–60. doi:https://doi.org/10.1016/B978-0-444-63436-8.00002-8.

[9] C.C. Hinckley, Paramagnetic shifts in solutions of cholesterol and the dipyridine adduct of trisdipivalomethanatoeuropium(III). A shift reagent, J. Am. Chem. Soc. 91 (1969) 5160–5162. doi:10.1021/ja01046a038.

[10] B. Bleaney, Nuclear magnetic resonance shifts in solution due to lanthanide ions, J. Magn. Reson. 8 (1972) 91–100. doi:10.1016/0022-2364(72)90027-3.

[11] R.E. Sievers, R.E. Rondeau, New superior paramagnetic shift reagents for nuclear magnetic resonance spectral clarification, J. Am. Chem. Soc. 93 (1971) 1522–1524. doi:10.1021/ja00735a049.

[12] C.F.G.C. Geraldes, Lanthanides: Shift Reagents, in: Encycl. Inorg. Bioinorg. Chem., John Wiley & Sons, Ltd, Chichester, UK, 2012: pp. 1–20. doi:10.1002/9781119951438.eibc2050.

[13] G.R. Sullivan, Chiral Lanthanide Shift Reagents, in: Top. Stereochem., 2007: pp. 287–329. doi:10.1002/9780470147191.ch4.

[14] T.J. Wenzel, J.D. Wilcox, Chiral reagents for the determination of enantiomeric excess and absolute configuration using NMR spectroscopy, Chirality. 15 (2003) 256–270. doi:10.1002/chir.10190.

[15] I. Sengupta, P.S. Nadaud, C.P. Jaroniec, Protein structure determination with paramagnetic solid-state NMR spectroscopy, Acc. Chem. Res. 46 (2013) 2117–2126. doi:10.1021/ar300360q.

[16] C.P. Jaroniec, Structural studies of proteins by paramagnetic solid-state NMR spectroscopy, J. Magn. Reson. 253 (2015) 50–59. doi:10.1016/j.jmr.2014.12.017.

[17] A.D. Sherry, C.R. Malloy, F.M.H. Jeffrey, W.P. Cacheris, C.F.G.C. Geraldes, Dy(DOTP)5-: A new, stable 23Na shift reagent, J. Magn. Reson. 76 (1988) 528–533. doi:10.1016/0022-2364(88)90354-X.

[18] P. Harvey, A.M. Blamire, J.I. Wilson, K.-L.N.A. Finney, A.M. Funk, P.K. Senanayake, D. Parker, Moving the goal posts: enhancing the sensitivity of PARASHIFT proton magnetic resonance imaging and spectroscopy, Chem. Sci. 4 (2013) 4251. doi:10.1039/c3sc51526e.

[19] M. Woods, D.E. Woessner, A.D. Sherry, Paramagnetic lanthanide complexes as PARACEST agents for medical imaging, Chem. Soc. Rev. 35 (2006) 500. doi:10.1039/b509907m.

[20] L.M. De Leon-Rodriguez, A.J.M. Lubag, C.R. Malloy, G. V. Martinez, R.J. Gillies, A.D. Sherry, Responsive MRI agents for sensing metabolism in vivo, Acc. Chem. Res. 42 (2009) 948–957. doi:10.1021/ar800237f.

[21] S. Viswanathan, Z. Kovacs, K.N. Green, S.J. Ratnakar, A.D. Sherry, Alternatives to Gadolinium-Based Metal Chelates for Magnetic Resonance Imaging †, Chem. Rev. 110 (2010) 2960–3018. doi:10.1021/cr900284a.

[22] D. Parker, I. Kuprov, E. Suturina, K. Mason, C. Geraldes, Beyond Bleaney's Theory: Experimental and Theoretical Analysis of Periodic Trends in Lanthanide Induced Chemical Shift, Angew. Chemie Int. Ed. (2017) 12215–12218. doi:10.1002/anie.201706931.

[23] A.M. Funk, K.-L.N.A. Finney, P. Harvey, A.M. Kenwright, E.R. Neil, N.J. Rogers, P.K. Senanayake, D. Parker, Critical analysis of the limitations of Bleaney's theory of magnetic anisotropy in paramagnetic lanthanide coordination complexes, Chem. Sci. 6 (2015) 1655–1662. doi:10.1039/c4sc03429e.

[24] W. Van den Heuvel, A. Soncini, NMR chemical shift as analytical derivative of the Helmholtz free energy, J. Chem. Phys. 138 (2013) 054113. doi:10.1063/1.4789398.
[25] J. Autschbach, S. Patchkovskii, B. Pritchard, Calculation of hyperfine tensors and paramagnetic NMR shifts using the relativistic zeroth-order regular approximation and density functional theory, J. Chem. Theory Comput. 7 (2011) 2175–2188. doi:10.1021/ct200143w.
[26] A. V. Arbuznikov, J. Vaara, M. Kaupp, Relativistic spin-orbit effects on hyperfine coupling tensors by density-functional theory, J. Chem. Phys. 120 (2004) 2127–2139. doi:10.1063/1.1636720.
[27] H. Liimatainen, T.O. Pennanen, J. Vaara, 1 H chemical shifts in nonaxial, paramagnetic chromium(III) complexes — Application of novel pNMR shift theory, Can. J. Chem. 87 (2009) 954–964. doi:10.1139/V09-045.
[28] M. Vonci, K. Mason, E.A. Suturina, A.T. Frawley, S.G. Worswick, I. Kuprov, D. Parker, E.J.L. Mcinnes, N.F. Chilton, Rationalization of Anomalous Pseudocontact Shifts and Their Solvent Dependence in a Series of C 3 - Symmetric Lanthanide Complexes, (2017). doi:10.1021/jacs.7b07094.
[29] A.D. Sherry, P. Caravan, R.E. Lenkinski, Primer on gadolinium chemistry, J. Magn. Reson. Imaging. 30 (2009) 1240–1248. doi:10.1002/jmri.21966.
[30] K. Mason, N.J. Rogers, E.A. Suturina, I. Kuprov, J.A. Aguilar, A.S. Batsanov, D.S. Yufit, D. Parker, PARASHIFT Probes: Solution NMR and X-ray Structural Studies of Macrocyclic Ytterbium and Yttrium Complexes, Inorg. Chem. 56 (2017) 4028–4038. doi:10.1021/acs.inorgchem.6b02291.
[31] K.H. Chalmers, A.M. Kenwright, D. Parker, A.M. Blamire, 19F-lanthanide complexes with increased sensitivity for 19F-MRI: Optimization of the MR acquisition, Magn. Reson. Med. 66 (2011) 931–936. doi:10.1002/mrm.22881.
[32] A.M. Funk, P.H. Fries, P. Harvey, A.M. Kenwright, D. Parker, Experimental measurement and theoretical assessment of fast lanthanide electronic relaxation in solution with four series of isostructural complexes, J. Phys. Chem. A. 117 (2013) 905–917. doi:10.1021/jp311273x.
[33] S. Aime, M. Botta, M. Fasano, E. Terreno, P. Kinchesh, L. Calabi, L. Paleari, A new ytterbium chelate as contrast agent in chemical shift imaging and temperature sensitive probe for MR spectroscopy, Magn. Reson. Med. 35 (1996) 648–651. doi:10.1002/mrm.1910350504.
[34] S.K. Hekmatyar, P. Hopewell, S.K. Pakin, A. Babsky, N. Bansal, Noninvasive MR thermometry using paramagnetic lanthanide complexes of 1,4,7,10-tetraazacyclododecane-α,α′,α″,α‴-tetramethyl-1,4,7,10-tetraacetic acid (DOTMA4-), Magn. Reson. Med. 53 (2005) 294–303. doi:10.1002/mrm.20345.
[35] R. Schmidt, N. Nippe, K. Strobel, M. Masthoff, O. Reifschneider, D.D. Castelli, C. Holtke, S. Aime, U. Karst, C. Sunderkotter, C. Bremer, C. Faber, Highly shifted proton MR imaging: cell tracking by using direct detection of paramagnetic compounds, Radiology. 272 (2014) 785–795. doi:10.1148/radiol.14132056.
[36] O.A. Blackburn, R.M. Edkins, S. Faulkner, A.M. Kenwright, D. Parker, N.J. Rogers, S. Shuvaev, Electromagnetic susceptibility anisotropy and its importance for paramagnetic NMR and optical spectroscopy in lanthanide coordination chemistry, Dalt. Trans. 45 (2016) 6782–6800. doi:10.1039/C6DT00227G.
[37] N.J. Rogers, K.-L.N.A. Finney, P.K. Senanayake, D. Parker, Another challenge to paramagnetic relaxation theory: a study of paramagnetic proton NMR relaxation in closely related series of pyridine-derivatised dysprosium complexes, Phys. Chem. Chem. Phys. 18 (2016) 4370–4375. doi:10.1039/C5CP06755C.
[38] P.K. Senanayake, N.J. Rogers, K.-L.N.A. Finney, P. Harvey, A.M. Funk, J.I. Wilson, D. O'Hogain, R. Maxwell, D. Parker, A.M. Blamire, A new paramagnetically shifted imaging probe for MRI, Magn. Reson. Med. 77 (2017) 1307–1317. doi:10.1002/mrm.26185.
[39] D. Coman, H.K. Trubel, R.E. Rycyna, F. Hyder, Brain temperature and pH measured by 1H chemical shift imaging of a thulium agent, NMR Biomed. 22 (2009) 229–239. doi:10.1002/nbm.1312.
[40] D. Coman, H.K. Trubel, F. Hyder, Brain temperature by Biosensor Imaging of Redundant Deviation in Shifts (BIRDS): Comparison between TmDOTP5- and TmDOTMA-, NMR Biomed. 23 (2010) 277–285. doi:10.1002/nbm.1461.
[41] D. Coman, R.A. de Graaf, D.L. Rothman, F. Hyder, In vivo three-dimensional molecular imaging with Biosensor Imaging of Redundant Deviation in Shifts (BIRDS) at high spatiotemporal resolution, NMR Biomed. 26 (2013) 1589–1595. doi:10.1002/nbm.2995.
[42] D. Coman, Y. Huang, J.U. Rao, H.M. De Feyter, D.L. Rothman, C. Juchem, F. Hyder, Imaging the intratumoral-peritumoral extracellular pH gradient of gliomas, NMR Biomed. 29 (2016) 309–319. doi:10.1002/nbm.3466.
[43] Y. Huang, D. Coman, P. Herman, J.U. Rao, S. Maritim, F. Hyder, Towards longitudinal mapping of extracellular pH in gliomas, NMR Biomed. 29 (2016) 1364–1372. doi:10.1002/nbm.3578.
[44] S.K. Pakin, S.K. Hekmatyar, P. Hopewell, A. Babsky, N. Bansal, Non-invasive temperature imaging with

thulium 1,4,7, 10-tetraazacyclododecane- 1,4,7, 10-tetramethyl-1,4,7, 10-tetraacetic acid (TmDOTMA-), NMR Biomed. 19 (2006) 116–124. doi:10.1002/nbm.1010.
[45] J.R. James, Y. Gao, M.A. Miller, A. Babsky, N. Bansal, Absolute temperature MR imaging with thulium 1,4,7,10- tetraazacyclododecane-1,4,7,10-tetramethyl-1,4,7,10-tetraacetic acid (TmDOTMA-), Magn. Reson. Med. 62 (2009) 550–556. doi:10.1002/mrm.22039.
[46] K.-L.N.A. Finney, A.C. Harnden, N.J. Rogers, P.K.K. Senanayake, A.M. Blamire, D. O'Hogain, D. Parker, Simultaneous Triple Imaging with Two PARASHIFT Probes: Encoding Anatomical, pH and Temperature Information using Magnetic Resonance Shift Imaging, Chem. - A Eur. J. 23 (2017) 7976–7989. doi:10.1002/chem.201700447.
[47] J.C. Hindman, Proton Resonance Shift of Water in the Gas and Liquid States, J. Chem. Phys. 44 (1966) 4582–4592. doi:10.1063/1.1726676.
[48] B. Quesson, J.A. de Zwart, C.T.W. Moonen, Magnetic resonance temperature imaging for guidance of thermotherapy, J. Magn. Reson. Imaging. 12 (2000) 525–533. doi:10.1002/1522-2586(200010)12:4<525::AID-JMRI3>3.0.CO;2-V.
[49] C. Weidensteiner, B. Quesson, B. Caire-Gana, N. Kerioui, A. Rullier, H. Trillaud, C.T.W. Moonen, Real-time MR temperature mapping of rabbit liver in vivo during thermal ablation, Magn. Reson. Med. 50 (2003) 322–330. doi:10.1002/mrm.10521.
[50] T. Frenzel, K. Roth, S. Koßler, B. Radüchel, H. Bauer, J. Platzek, H.-J. Weinmann, Noninvasive temperature measurement in Vivo using a temperature-sensitive lanthanide complex and 1H magnetic resonance spectroscopy, Magn. Reson. Med. 35 (1996) 364–369. doi:10.1002/mrm.1910350314.
[51] K. Roth, G. Bartholomae, H. Bauer, T. Frenzel, S. Kossler, J. Platzek, H.-J. Weinmann, Pr[MOE-DO3A], a Praseodymium Complex of a Tetraazacyclododecane: An In Vivo NMR Thermometer, Angew. Chem. Int. Ed. 35 (1996) 655–657. doi:10.1002/anie.199606551.
[52] M. Hentschel, P. Wust, W. Wlodarczyk, T. Frenzel, B. Sander, N. Hosten, R. Felix, Non-invasive MR thermometry by 2D spectroscopic imaging of the Pr[MOE-DO3A] complex, Int. J. Hyperth. 14 (1998) 479–493. doi:10.3109/02656739809018249.
[53] M. Hentschel, W. Dreher, P. Wust, S. Röll, D. Leibfritz, R. Felix, S. Roll, D. Leibfritz, R. Felix, S. Röll, D. Leibfritz, R. Felix, Fast spectroscopic imaging for non-invasive thermometry using the Pr[MOE-DO3A] complex, Phys. Med. Biol. 44 (1999) 2397–2408. doi:10.1088/0031-9155/44/10/303.
[54] M. Hentschel, M. Findeisen, W. Schmidt, T. Frenzel, W. Wlodarczyk, P. Wust, R. Felix, Is absolute noninvasive temperature measurement by the Pr[MOE-DO3A] complex feasible, Magn. Reson. Mater. Physics, Biol. Med. 10 (2000) 52–59. doi:10.1016/S1352-8661(99)00075-7.
[55] C.C. Heyn, J. Bishop, K. Duffin, W. Lee, J. Dazai, S. Spring, B.J. Nieman, J.G. Sled, Magnetic resonance thermometry of flowing blood, NMR Biomed. (2017) e3772. doi:10.1002/nbm.3772.
[56] V.S. Mironov, Y.G. Galyametdinov, A. Ceulemans, C. Görller-Walrand, K. Binnemans, Room-temperature magnetic anisotropy of lanthanide complexes: A model study for various coordination polyhedra, J. Chem. Phys. 116 (2002) 4673–4685. doi:10.1063/1.1450543.
[57] C.S. Zuo, J.L. Bowers, K.R. Metz, T. Nosaka, a D. Sherry, M.E. Clouse, TmDOTP5-: a substance for NMR temperature measurements in vivo., Magn. Reson. Med. 36 (1996) 955–9. doi:10.1002/mrm.1910360619.
[58] A. Dean Sherry, MR imaging and spectroscopy applications of lanthanide complexes with macrocyclic phosphonate and phosphonate ester ligands, J. Alloys Compd. 249 (1997) 153–157. doi:10.1016/S0925-8388(96)02518-2.
[59] C.S. Zuo, A. Mahmood, A.D. Sherry, TmDOTA − : A Sensitive Probe for MR Thermometry in Vivo, J. Magn. Reson. 151 (2001) 101–106. doi:10.1006/jmre.2001.2356.
[60] S.K. Hekmatyar, H. Poptani, A. Babsky, D.B. Leeper, N. Bansal, Non-invasive magnetic resonance thermometry using thulium-1,4,7,10- tetraazacyclododecane-1,4,7,10-tetraacetate (TmDOTA-), Int. J. Hyperth. 18 (2002) 165–179. doi:10.1080/0265673011009859.
[61] S. Aime, A. Barge, D.D. Castelli, F. Fedeli, A. Mortillaro, F.U. Nielsen, E. Terreno, Paramagnetic lanthanide(III) complexes as pH-sensitive chemical exchange saturation transfer (CEST) contrast agents for MRI applications, Magn. Reson. Med. 47 (2002) 639–648. doi:10.1002/mrm.10106.
[62] S. Zhang, A.D. Sherry, Physical characteristics of lanthanide complexes that act as magnetization transfer (MT) contrast agents, J. Solid State Chem. 171 (2003) 38–43. doi:10.1016/S0022-4596(02)00143-3.
[63] D. Coman, G.E. Kiefer, D.L. Rothman, A.D. Sherry, F. Hyder, A lanthanide complex with dual biosensing properties: CEST (chemical exchange saturation transfer) and BIRDS (biosensor imaging of redundant deviation in shifts) with europium DOTA-tetraglycinate, NMR Biomed. 24 (2011) 1216–1225. doi:10.1002/nbm.1677.

[64] S. Aime, M. Botta, L. Milone, E. Terreno, Paramagnetic complexes as novel NMR pH indicators, Chem. Commun. (1996) 1265–1266. doi:10.1039/cc9960001265.
[65] C.S. Zuo, K.R. Metz, Y. Sun, A.D. Sherry, NMR Temperature Measurements Using a Paramagnetic Lanthanide Complex, J. Magn. Reson. 133 (1998) 53–60. doi:10.1006/jmre.1998.1429.
[66] Y. Sun, M. Sugawara, R. V. Mulkern, K. Hynynen, S. Mochizuki, M. Albert, C.S. Zuo, Simultaneous measurements of temperature and pHin vivo using NMR in conjunction with TmDOTP5?, NMR Biomed. 13 (2000) 460–466. doi:10.1002/nbm.676.
[67] H.K.F. Trübel, P.K. Maciejewski, J.H. Farber, F. Hyder, Brain temperature measured by 1 H-NMR in conjunction with a lanthanide complex, J. Appl. Physiol. 94 (2003) 1641–1649. doi:10.1152/japplphysiol.00841.2002.
[68] H.K.F. Trubel, P.K. Maciejewski, J.H. Farbe, F. Hyder, Brain thermometry by 1H MRS using a thulium-based shift reagent (TmDOTP^5-), Magn. Reson. Med. 1 (2002) 95173.
[69] J.U. Rao, D. Coman, J.J. Walsh, M.M. Ali, Y. Huang, F. Hyder, Temozolomide arrests glioma growth and normalizes intratumoral extracellular pH, Sci. Rep. 7 (2017) 7865. doi:10.1038/s41598-017-07609-7.
[70] S. Zhang, K. Wu, A.D. Sherry, A Novel pH-Sensitive MRI Contrast Agent, Angew. Chemie Int. Ed. 38 (1999) 3192–3194. doi:10.1002/(SICI)1521-3773(19991102)38:21<3192::AID-ANIE3192>3.0.CO;2-#.
[71] N. Raghunand, C. Howison, A.D. Sherry, S. Zhang, R.J. Gillies, Renal and systemic pH imaging by contrast-enhanced MRI, Magn. Reson. Med. 49 (2003) 249–257. doi:10.1002/mrm.10347.
[72] M.L. Garcia-Martin, G. V. Martinez, N. Raghunand, A.D. Sherry, S. Zhang, R.J. Gillies, High resolution pHe imaging of rat glioma using pH-dependent relaxivity, Magn. Reson. Med. 55 (2006) 309–315. doi:10.1002/mrm.20773.
[73] Y. Huang, D. Coman, M.M. Ali, F. Hyder, Lanthanide ion (III) complexes of 1,4,7,10-tetraazacyclododecane-1,4,7,10-tetraaminophosphonate for dual biosensing of pH with chemical exchange saturation transfer (CEST) and biosensor imaging of redundant deviation in shifts (BIRDS), Contrast Media Mol. Imaging. 10 (2015) 51–58. doi:10.1002/cmmi.1604.
[74] S. Maritim, Y. Huang, D. Coman, F. Hyder, Characterization of a lanthanide complex encapsulated with MRI contrast agents into liposomes for biosensor imaging of redundant deviation in shifts (BIRDS), J. Biol. Inorg. Chem. 19 (2014) 1385–1398. doi:10.1007/s00775-014-1200-z.
[75] E. De Luca, P. Harvey, K.H. Chalmers, A. Mishra, P.K. Senanayake, J.I. Wilson, M. Botta, M. Fekete, A.M. Blamire, D. Parker, Characterisation and evaluation of paramagnetic fluorine labelled glycol chitosan conjugates for 19F and 1H magnetic resonance imaging Topical Issue on Metal-Based MRI Contrast Agents. Guest editor: Valerie C. Pierre, J. Biol. Inorg. Chem. 19 (2014) 215–227. doi:10.1007/s00775-013-1028-y.
[76] Y. Huang, D. Coman, F. Hyder, M.M. Ali, Dendrimer-Based Responsive MRI Contrast Agents (G1-G4) for Biosensor Imaging of Redundant Deviation in Shifts (BIRDS), Bioconjug. Chem. 26 (2015) 2315–2323. doi:10.1021/acs.bioconjchem.5b00568.
[77] J. Rena, A.D. Sherry, 7Li, 6Li, 23Na and 133Cs multinuclear NMR studies of adducts formed with shift reagent, TmDOTP5, Inorg Chim. Acta. 246 (1996) 331–341. doi:10.1016/0020-1693(96)05080-3.
[78] N. Bansal, M.J. Germann, V. Seshan, G.T. Shires III, C.R. Malloy, A.D. Sherry, Thulium 1,4,7,10-tetraazacyclododecane-1,4,7,10-tetrakis(methylene phosphonate) as a sodium-23 shift reagent for the in vivo rat liver, Biochemis. 32 (1993) 5638–5643. doi:10.1021/bi00072a020.
[79] M. Milne, R.H.E. Hudson, Contrast agents possessing high temperature sensitivity, Chem. Commun. 47 (2011) 9194. doi:10.1039/c1cc13073k.
[80] P. Marckmann, L. Skov, K. Rossen, A. Dupont, M. Brimnes Damholt, J. Goya Heaf, H.S. Thomsen, Nephrogenic Systemic Fibrosis: Suspected Causative Role of Gadodiamide Used for Contrast-Enhanced Magnetic Resonance Imaging, J. Am. Soc. Nephrol. 17 (2006) 2359–2362. doi:10.1681/ASN.2006060601.
[81] EMA's final opinion confirms restrictions on use of linear gadolinium agents in body scans, European Medicines Agency, 2017.
[82] F. Touti, P. Maurin, J. Hasserodt, Magnetogenesis under physiological conditions with probes that report on (Bio-)chemical stimuli, Angew. Chemie - Int. Ed. 52 (2013) 4654–4658. doi:10.1002/anie.201208848.
[83] E.M. Gale, I.P. Atanasova, F. Blasi, I. Ay, P. Caravan, A Manganese Alternative to Gadolinium for MRI Contrast, J. Am. Chem. Soc. 137 (2015) 15548–15557. doi:10.1021/jacs.5b10748.
[84] H. Wei, O.T. Bruns, M.G. Kaul, E.C. Hansen, M. Barch, A. Wiśniowska, O. Chen, Y. Chen, N. Li, S. Okada, J.M. Cordero, M. Heine, C.T. Farrar, D.M. Montana, G. Adam, H. Ittrich, A. Jasanoff, P. Nielsen, M.G. Bawendi, Exceedingly small iron oxide nanoparticles as positive MRI contrast agents, Proc. Natl. Acad. Sci. 114 (2017) 2325–2330. doi:10.1073/pnas.1620145114.

[85] P.B. Tsitovich, J.R. Morrow, Macrocyclic ligands for Fe(II) paraCEST and chemical shift MRI contrast agents, Inorganica Chim. Acta. 393 (2012) 3–11. doi:10.1016/j.ica.2012.06.010.
[86] P.B. Tsitovich, J.M. Cox, J.B. Benedict, J.R. Morrow, Six-coordinate Iron(II) and Cobalt(II) paraSHIFT Agents for Measuring Temperature by Magnetic Resonance Spectroscopy, Inorg. Chem. 55 (2016) 700–716. doi:10.1021/acs.inorgchem.5b02144.
[87] P.B. Tsitovich, T.Y. Tittiris, J.M. Cox, J.B. Benedict, J.R. Morrow, Fe(II) and Co(II) N-methylated CYCLEN complexes as paraSHIFT agents with large temperature dependent shifts, Dalt. Trans. 47 (2018) 916–924. doi:10.1039/C7DT03812G.
[88] S. Aime, M. Botta, G. Ermondi, NMR study of solution structures and dynamics of lanthanide(III) complexes of DOTA, Inorg. Chem. 31 (1992) 4291–4299. doi:10.1021/ic00047a016.
[89] E.S. O'Neill, J.L. Kolanowski, P.D. Bonnitcha, E.J. New, A cobalt(II) complex with unique paraSHIFT responses to anions, Chem. Commun. 53 (2017) 3571–3574. doi:10.1039/C7CC00619E.
[90] I. Bertini, C. Luchinat, G. Parigi, E. Ravera, Chapter 7 - Transition metal ions: shift and relaxation, in: I. Bertini, C. Luchinat, G. Parigi, E. Ravera (Eds.), NMR Paramagn. Mol. (Second Ed., Second Edi, Elsevier, Boston, 2017: pp. 175–253. doi:https://doi.org/10.1016/B978-0-444-63436-8.00008-9.
[91] M. Atanasov, D. Aravena, E. Suturina, E. Bill, D. Maganas, F. Neese, First principles approach to the electronic structure, magnetic anisotropy and spin relaxation in mononuclear 3d-transition metal single molecule magnets, Coord. Chem. Rev. 289–290 (2015) 177–214. doi:10.1016/j.ccr.2014.10.015.
[92] B. Martin, J. Autschbach, Temperature dependence of contact and dipolar NMR chemical shifts in paramagnetic molecules, J. Chem. Phys. 142 (2015). doi:10.1063/1.4906318.
[93] A.J. Pell, G. Pintacuda, C.P. Grey, Paramagnetic NMR in solution and the solid state, Prog. Nucl. Magn. Reson. Spectrosc. (2018). doi:10.1016/j.pnmrs.2018.05.001.